

Adaptive Graph Auto-Encoder for General Data Clustering

Xuelong Li, Hongyuan Zhang, Rui Zhang

School of Computer Science and School of Artificial Intelligence, Optics and Electronics (iOPEN),
Northwestern Polytechnical University, Xi'an 710072, Shaanxi, P. R. China

xuelong_li@nwpu.edu.cn, hyzhang98@gmail.com, ruizhang8633@gmail.com

Abstract

*Graph-based clustering plays an important role in the clustering area. Recent studies about graph convolution neural networks have achieved impressive success on graph type data. However, in general clustering tasks, the graph structure of data does not exist such that the strategy to construct a graph is crucial for performance. Therefore, how to extend graph convolution networks into general clustering tasks is an attractive problem. In this paper, we propose a graph auto-encoder for general data clustering, which constructs the graph adaptively according to the generative perspective of graphs. The adaptive process is designed to induce the model to exploit the high-level information behind data and utilize the non-Euclidean structure sufficiently. We further design a novel mechanism with rigorous analysis to avoid the collapse caused by the adaptive construction. Via combining the generative model for network embedding and graph-based clustering, a graph auto-encoder with a novel decoder is developed such that it performs well in weighted graph used scenarios. Extensive experiments prove the superiority of our model.*¹

1. Introduction

Clustering, which intends to group data points without any prior information, is one of the most fundamental tasks in machine learning. As well as the well-known k-means, graph-based clustering [21, 22, 42] is also a representative kind of clustering method. Graph-based clustering methods can capture manifold information so that they are available for the non-Euclidean type data, which is not provided by k-means. Therefore, they are widely used in practice. Due to the success of deep learning, how to combine neural networks and traditional clustering models has been studied a lot [30, 37, 41]. In particular, CNN-based clustering models have been extensively investigated [8, 39, 40]. However, the convolution operation may be unavailable on other kinds of

datasets, *e.g.*, text datasets, social network datasets, *etc.*

Network embedding is a fundamental task for graph type data such as recommendation systems, social networks, *etc.* The goal is to map nodes of a given graph into latent features (namely embedding) such that the learned embedding can be utilized on node classification, node clustering, and link prediction. Roughly speaking, the network embedding approaches can be classified into 2 categories: generative models [9, 27, 35] and discriminative models [4, 34]. The former tries to model a connectivity distribution for each node while the latter learns to distinguish whether an edge exists between two nodes directly.

In recent years, graph neural networks (GNN) [29], especially graph convolution neural networks (GCN), have attracted a mass of attention due to the success made in the neural networks area. GNNs extend classical neural networks into irregular data so that the deep information hidden in graphs is exploited sufficiently. In this paper, we only focus on GCNs and its variants. GCNs have shown superiority compared with traditional network embedding models. Similarly, graph auto-encoder (GAE) [15] is developed to extend GCN into unsupervised learning.

However, the existing methods are limited to graph type data while no graph is provided for general data clustering. Since a large proportion of clustering methods are based on the graph, it is reasonable to consider how to employ GCN to promote the performance of graph-based clustering methods. In this paper, we propose an Adaptive Graph Auto-Encoder to extend graph auto-encoder into common scenarios. The main contributions are listed as follows:

- To build a desirable graph, our model incorporates generative models of network embedding. Based on the generative perspective, the representation learning is further integrated such that the graph auto-encoder is naturally employed to learn embedding.
- The learned connectivity distribution, obtained from the generative graph models, is used as the goal that graph auto-encoder aims to reconstruct, which also inspires us to devise a novel architecture for decoders.

¹The codes of AdaGAE can be downloaded from <https://github.com/hyzhang98/AdaGAE>.

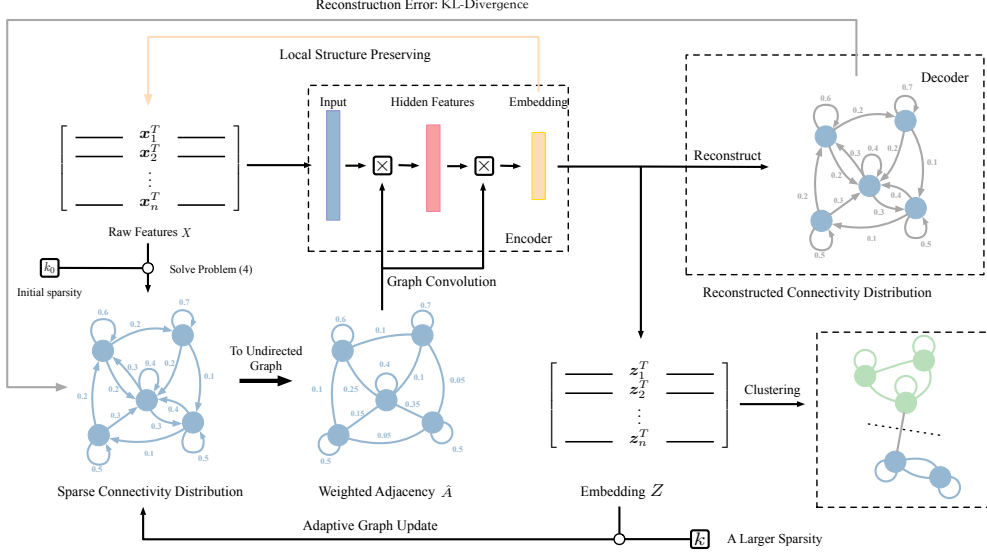


Figure 1. Framework of AdaGAE. k_0 is the initial sparsity. First, we construct a sparse graph via the generative model defined in Eq. (21). The learned graph is employed to apply the GAE designed for the weighted graphs. After training the GAE, we update the graph from the learned embedding with a larger sparsity, k . With the new graph, we re-train the GAE. These steps are repeated until the convergence.

- Our model updates the graph adaptively according to the generated embedding such that it can exploit the deep information and revise the poor graph caused by raw features. We eliminate the collapse caused by the adaptive construction via changing the sparsity of the graph. Besides, the related theoretical analyses are given to understand the collapse phenomenon.

2. Preliminary and Related Work

2.1. Notations

In this paper, matrices and vectors are represented by uppercase and lowercase letters respectively. A graph is represented as $\mathcal{G} = (\mathcal{V}, \mathcal{E}, \mathcal{W})$ and $|\cdot|$ is the size of some set. Vectors whose all elements equal 1 are represented as $\mathbf{1}$. If $\langle v_i, v_j \rangle \in \mathcal{E}$, then $\mathcal{W}_{ij} > 0$; otherwise, $\mathcal{W}_{ij} = 0$. For every node $v_i \in \mathcal{V}$, it is represented by a d -dimension vector \mathbf{x}_i and thus, \mathcal{V} can be also denoted by $X = [\mathbf{x}_1, \mathbf{x}_2, \dots, \mathbf{x}_n]^T \in \mathbb{R}^{n \times d}$. The amount of data points and clusters are represented as n and c respectively. All proofs are shown in supplementary.

2.2. Deep Clustering

An important topic in clustering field is deep clustering, which utilizes neural networks to enhance the capacity of model. A fundamental model is auto-encoder (AE) [12], which has been widely used in diverse clustering methods [19, 26, 37, 41]. Besides the AE-based models, SpectralNet [30] attempts to transform the core idea of spectral clustering to neural networks. In image clustering fields, CNN-based models have achieved impressive performance. For instance, JULE [39] employs both CNN and RNN to

obtain better representation. DEPICT [8] and deep spectral clustering with dual networks [40] are based on convolution auto-encoders. However, they can only be applied on image datasets. Since we focus on clustering on both regular and irregular data, **these CNN-based models will not be regarded as main competitors.**

2.3. Graph Auto-Encoder

In recent years, GCNs have been studied a lot to extend neural networks to graph type data. How to design a graph convolution operator is a key issue and has attracted a mass of attention. Most of them can be classified into 2 categories, spectral methods [23] and spatial methods [3]. In this paper, we focus on a simple but widely used convolution operator [16], which can be regarded as both the spectral operator and spatial operator. Formally, if the input of a graph convolution layer is $X \in \mathbb{R}^{n \times d}$ and the adjacency matrix is A , then the output is defined as

$$H = \varphi(\hat{A}XW), \quad (1)$$

where $\varphi(\cdot)$ is certain activation function, $\hat{A} = \tilde{D}^{-\frac{1}{2}} \tilde{A} \tilde{D}^{-\frac{1}{2}}$, $\tilde{A} = A + I$, \tilde{D} denotes the degree matrix ($\tilde{D}_{ii} = \sum_{j=1}^n \tilde{A}_{ij}$), and W denotes the parameters of GCN. It should be pointed out that \tilde{A} is a graph with self-loop for each node and \hat{A} is the normalized adjacency matrix. More importantly, $\hat{A}X$ is equivalent to compute weighted means for each node with its first-order neighbors from the spatial aspect. To improve the performance, MixHop [1] aims to mix information from different order neighbors and SGC [36] tries to utilize higher-order neighbors. The capacity of GCN is also proved to some extent [38]. GCN and its vari-

ants are usually used on semi-supervised learning. Besides, since the training of each GCN layer needs all data to finish a complete propagation, several models are proposed to speed it up [5, 6].

To apply graph convolution on unsupervised learning, GAE is proposed [15]. GAE firstly transforms each node into latent representation (namely embedding), which is similar to GCN, and then aims to reconstruct some part of the input. GAEs proposed in [15, 24, 32] intend to reconstruct the adjacency via decoder while GAEs developed in [33] attempt to reconstruct the content. The difference is which extra mechanism (such as attention, adversarial learning, graph sharpness, *etc.*) is used.

3. Proposed Model

In this section, we will show the proposed model, Adaptive Graph Auto-Encoder (*AdaGAE*) for general data clustering. The core idea is illustrated in Figure 1.

3.1. Probabilistic Perspective of Weighted Graphs

In this paper, the underlying connectivity distribution of node v_i is denoted by conditional probability $p(v|v_i)$ such that $\sum_{j=1}^n p(v_j|v_i) = 1$. From this perspective, a link can be regarded as a sampling result according to $p(v|v_i)$, which is the core assumption of the generative network embedding.

In general clustering scenarios, links between two nodes frequently do not exist. Therefore, we need to construct a weighted graph via some scheme. Since $p(v_j|v_i) \geq 0$, the probability can be regarded as valid weights. Note that $p(v_j|v_i) \neq p(v_i|v_j)$ usually holds, and therefore, the constructed graph should be viewed as a directed graph. Therefore, the construction of the weighted graph is equivalent to finding the underlying connectivity distribution. The following assumption helps us to find an approximate connectivity distribution,

Assumption 1. *In an ideal situation, the representation of v_i is analogous to the one of v_j if $p(v_i|v_j)$ is large.*

Suppose that divergence between v_i and v_j is denoted by

$$d(v_i, v_j) = \|f(\mathbf{x}_i) - f(\mathbf{x}_j)\|_2^2, \quad (2)$$

where \mathbf{x}_i is the raw feature that describes the node v_i and $f(\cdot)$ is a mapping that aims to find the optimal representation to cater for Assumption 1. Accordingly, we expect that

$$\min_{p(\cdot|v_i), f(\cdot)} \sum_{i=1}^n \mathbb{E}_{v_j \sim p(\cdot|v_i)} d(v_i, v_j) = \sum_{i=1}^n \sum_{j=1}^n p(v_j|v_i) \cdot d_{ij}, \quad (3)$$

where $d_{ij} = d(v_i, v_j)$ for simplicity. To solve the above problem, the *alternative method* is utilized. However, it is

impracticable to solve the above problem directly, as its sub-problem regarding $p(\cdot|v_i)$ has a trivial solution: $p(v_i|v_i) = 1$ and $p(v_j|v_i) = 0$ if $j \neq i$. A universal method is to employ *Regularization Loss Minimization*, and the objective is given as

$$\min_{p(\cdot|v_i), f(\cdot)} \sum_{i=1}^n \mathbb{E}_{v_j \sim p(\cdot|v_i)} d_{ij} + \mathcal{R}(p(\cdot|v_i)), \quad (4)$$

where $\mathcal{R}(\cdot)$ is some regularization term. In metric learning and manifold learning, although the global distance is usually unreliable, the local distance [11, 28, 31] is frequently regarded as a vital part. Similarly, an ideal distribution should be sparse so that it can ignore the significantly different nodes. From another aspect, a graph is usually sparse and thus, $p(v|v_i)$ should be 0 for most nodes. Formally, let $\mathbf{p}_i = [p(v_1|v_i), p(v_2|v_i), \dots, p(v_n|v_i)]$ and the sparse distribution should satisfy that $\|\mathbf{p}_i\|_0 \leq s$ where s represents a small integer. Hence, the regularization term should be $\gamma \|\mathbf{p}_i\|_0$. Nevertheless, ℓ_0 -norm is non-convex and it is NP-hard to solve. Generally, we try to solve a convex ℓ_1 relaxation problem, *i.e.*, $\mathcal{R}(p(\cdot|v_i)) = \gamma \|\mathbf{p}_i\|_1$, since ℓ_1 -norm is the tightest convex relaxation of ℓ_0 -norm and it guarantees the sparseness of solution. However, the sparsity degree cannot be controlled precisely, *i.e.*, we need to tune the trade-off parameter γ manually. Theorem 5 shows that the ℓ_2 -norm relaxation can guarantee steerable sparsity. To control sparsity of distribution for each node, we utilize point-wise regularization.

Theorem 1. *The ℓ_2 -norm relaxation of problem (4) regarding $p(\cdot|v_i)$,*

$$\min_{p(\cdot|v_i)} \sum_{i=1}^n \mathbb{E}_{v_j \sim p(\cdot|v_i)} d_{ij} + \gamma_i \|\mathbf{p}_i\|_2^2, \quad (5)$$

has a k -sparse solution if γ_i satisfies

$$\frac{1}{2}(kd_{i \cdot}^{(k)} - \sum_{v=1}^k d_{i \cdot}^{(v)}) < \gamma_i \leq \frac{1}{2}(kd_{i \cdot}^{(k+1)} - \sum_{v=1}^k d_{i \cdot}^{(v)}). \quad (6)$$

where $d_{i \cdot}^{(v)}$ denotes the v -th smallest value of $\{d_{ij}\}_{j=1}^n$.

The point-wise regularization can control the sparsity of each node but also increase the amount of hyper-parameters. In this paper, we simply choose an identical sparsity for all nodes. Formally, γ_i is set as the upper bound for all nodes,

$$\gamma_i = \frac{1}{2}(kd_{i \cdot}^{(k+1)} - \sum_{v=1}^k d_{i \cdot}^{(v)}). \quad (7)$$

It should be emphasized that there is only one hyper-parameter, sparsity k , in our model, which is much easier to tune than the traditional ℓ_1 relaxation method. More importantly, we will show that problem (21) can be solved analytically in Section 3.6.

Algorithm 1 Algorithm to optimize AdaGAE

Input: Initial sparsity k_0 , the increment of sparsity t and number of iterations to update weight adjacency T .

$Z = X$, $k = k_0$.

for $i = 1, 2, \dots, T$ **do**

 Compute γ_i via Eq. (7).

 Compute $d_{ij} = \|z_i - z_j\|_2^2$.

 Compute $p(\cdot|v_i)$ and \hat{A} by solving problem (21) with k

repeat

 Update GAE with Eq. (11) by the gradient descent.

until convergence or exceeding maximum iterations.

 Get new embedding Z .

$k = k + t$.

end for

Perform spectral clustering on \hat{A} , or run k -means on Z .

Output: Clustering assignments.

3.2. Graph Auto-Encoder for Weighted Graph

In the last subsection, we only focus on how to obtain a sparse connectivity distribution with the fixed $f(\cdot)$. Here we concentrate on how to obtain $f(\cdot)$. In particular, a graph auto-encoder is employed as $f(\cdot)$ to utilize the estimated graph in this paper. After obtaining the connectivity distribution by solving problem (21), we transform the directed graph to an undirected graph via $\mathcal{W}_{ij} = (p(v_i|v_j) + p(v_j|v_i))/2$, and the connectivity distribution serves as the reconstruction goal of graph auto-encoder. Firstly, we elaborate details of the specific graph auto-encoder.

Encoder As shown in [16], graphs with self-loops show better performance, *i.e.*, $\tilde{A} = A + I$. Due to $d_{ii} = 0$, $p(v_i|v_i) \in (0, 1)$ if $k > 1$. Particularly, the weights of self-loops are learned adaptively rather than the primitive I . Consequently, we can simply set $\tilde{A} = \mathcal{W}$ and $\hat{A} = \tilde{D}^{-\frac{1}{2}} \tilde{A} \tilde{D}^{-\frac{1}{2}}$. The encoder consists of multiple GCN layers and aims to transform raw features to latent features with the constructed graph structure. Specifically speaking, the latent feature generated by m layers is defined as

$$Z = \varphi_m(\hat{A} \varphi_{m-1}(\dots \varphi_1(\hat{A} X W_1) \dots) W_m). \quad (8)$$

Decoder According to Assumption 1, we aim to recover the connectivity distribution $p(v|v_i)$ based on Euclidean distances, instead of reconstructing the weight matrix \tilde{A} via inner-products. Firstly, distances of latent features Z are calculated by $\hat{d}_{ij} = \|z_i - z_j\|_2^2$. Secondly, the connectivity distribution is reconstructed by a normalization step

$$q(v_j|v_i) = \frac{\exp(-\hat{d}_{ij})}{\sum_{j=1}^n \exp(-\hat{d}_{ij})}. \quad (9)$$

The above process can be regarded as inputting $-\hat{d}_{ij}$ into a SoftMax layer. Clearly, as \hat{d}_{ij} is smaller, $q(v_j|v_i)$ is larger. In other words, the similarity is measured by Euclidean distances rather than inner-products, which are usually used in GAE. To measure the difference between two distributions, Kullback-Leibler (KL) Divergence is therefore utilized and the objective function is defined as

$$\min_{q(\cdot|v_i)} KL(p||q) \Leftrightarrow \min_{q(\cdot|v_i)} \sum_{i,j=1}^n p(v_j|v_i) \log \frac{1}{q(v_j|v_i)}. \quad (10)$$

Note that it is equivalent to minimize the cross entropy, which is widely employed in classification tasks.

Loss Clearly, the representation provided by the graph auto-encoder can be used as a valid mapping, *i.e.*, $f(x_i) = z_i$. Therefore, the loss that integrates the graph auto-encoder and problem (4) is formulated as

$$\begin{aligned} & \min_{q,Z} KL(p||q) + \frac{\lambda}{2} \sum_{i=1}^n \mathbb{E}_{p(v_j|v_i)} \|z_i - z_j\|_2^2 + \gamma_i \|p_i\|_2^2 \\ & \Leftrightarrow \min_{q,Z} \sum_{i,j=1}^n p(v_j|v_i) \log \frac{1}{q(v_j|v_i)} + \frac{\lambda}{2} \sum_{i,j=1}^n \tilde{A}_{ij} \|z_i - z_j\|_2^2 \\ & \Leftrightarrow \min_{q,Z} \sum_{i,j=1}^n p(v_j|v_i) \log \frac{1}{q(v_j|v_i)} + \lambda \text{tr}(Z \tilde{L} Z^T), \end{aligned} \quad (11)$$

where $\tilde{L} = \tilde{D} - \tilde{A}$ and λ is a tradeoff parameter to balance the cross entropy term and local consistency penalty term.

3.3. Adaptive Graph Auto-Encoder

In the last subsection, the weighted adjacency matrix is viewed as fixed during training. However, the weighted adjacency matrix is computed by optimizing Eq. (21) at first. If the graph is not updated, then only the low-level information is utilized in GCN. The whole clustering process should contain connectivity learning and hence, the weighted adjacency should be updated adaptively during training. The adaptive evolution of the graph has two merits: 1) The model is induced to exploit the high-level information behind the data. The high-level information exploitation can be also regarded as a promotion of the GAE with shallow architecture. 2) It helps to correct the wrong links among samples that are caused by the low-level relationships.

A feasible approach is to recompute the connectivity distribution based on the embedding Z , which contains the potential manifold information of data. However, the following theorem shows that the simple update based on latent representations may lead to the collapse.

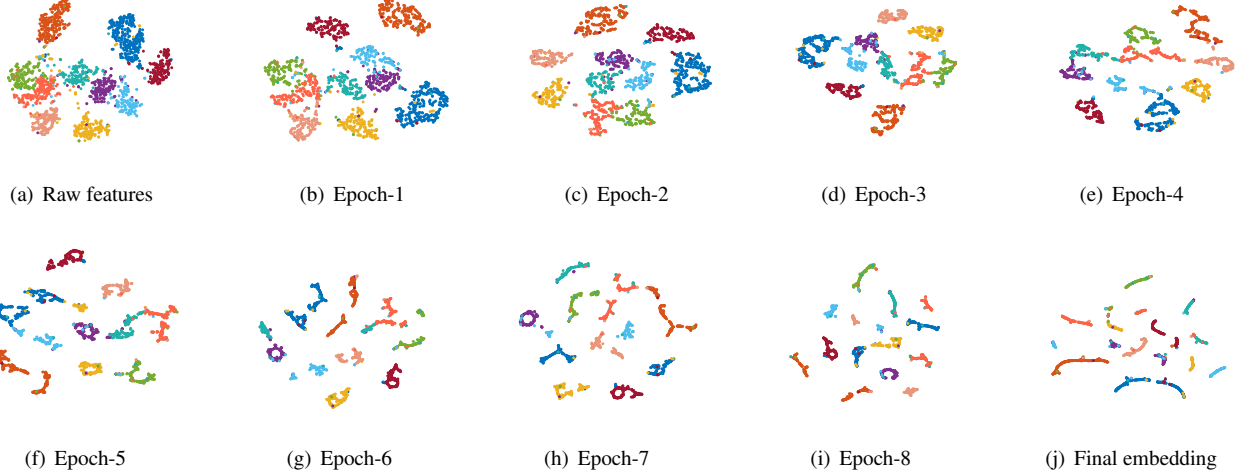


Figure 2. Visualization of the learning process of AdaGAE on USPS. Figure (b)-(i) show the embedding learned by AdaGAE at the i -th epoch, while the raw features and the final results are shown in Figure (a) and (j), respectively. An epoch corresponds to an update of the graph (given in Eq. (20)).

Theorem 2. Let $p^{(k)}(\cdot|v_i)$ be the k -largest $p(\cdot|v_i)$ and $\hat{d}_{ij} = \|z_i - z_j\|_2$ where z_i is generated by GAE with sparsity k . Let $\hat{p}(\cdot|v_i) = \arg \min_{p(\cdot|v_i)} \sum_{i=1}^n \mathbb{E}_{v_j \sim p(\cdot|v_i)} \hat{d}_{ij} + \gamma_i \|p_i\|_2^2$ where γ_i controls the sparsity as k . If $|q(\cdot|v_i) - p(\cdot|v_i)| \leq \varepsilon$ and $p^{(k)}(\cdot|v_i) \geq \sqrt{\varepsilon}$ (where $\varepsilon > 0$), then $\forall j, l \geq k$,

$$|\hat{p}^{(j)}(\cdot|v_i) - \hat{p}^{(l)}(\cdot|v_i)| \leq \frac{1}{k} \cdot \frac{1}{\frac{\log \varepsilon}{\log(\sqrt{\varepsilon} - \varepsilon)} - 1}. \quad (12)$$

Therefore, with $\varepsilon \rightarrow 0$, $\hat{p}(\cdot|v_i)$ will degenerate into a uniform distribution such that the weighted graph degenerates into an unweighted graph.

Intuitively, the unweighted graph is indeed a bad choice for clustering. Therefore, the update step with the same sparsity coefficient k may result in collapse. To address this problem, we assume that

Assumption 2. Suppose that the sparse and weighted adjacency contains sufficient information. Then, with latent representations, samples of an identical cluster become more cohesive measured by Euclidean distance.

According to the above assumption, samples from a cluster are more likely to lie in a local area after GAE mapping. Hence, the sparsity coefficient k increases when updating weight sparsity. The step size t which k increases with needs to be discussed. In an ideal situation, we can define the upper bound of k as

$$k_m^* = \min(|\mathcal{C}_1|, |\mathcal{C}_2|, \dots, |\mathcal{C}_c|), \quad (13)$$

where \mathcal{C}_i denotes the i -th cluster and $|\mathcal{C}_i|$ is the size of \mathcal{C}_i . Although $|\mathcal{C}_i|$ is not known, we can define k_m empirically

to ensure $k_m \leq k_m^*$. For instance, k_m can be set as $\lfloor \frac{n}{c} \rfloor$ or $\lfloor \frac{n}{2c} \rfloor$. Accordingly, the step size $t = \frac{k_m - k_0}{T}$ where T is the number of iterations to update the weight adjacency.

To sum up, Algorithm 1 summarizes the whole process to optimize AdaGAE.

3.3.1 Another Explanation of Degeneration

Theorem 3 demonstrates that the SoftMax output layer with $-\hat{d}_{ij}$ is equivalent to solve problem (4) with a totally different regularization. Overall, with the fixed k , better reconstructions mean the worse update. Therefore, the perfect reconstruction may lead to bad performance.

Theorem 3. The decoder of AdaGAE is equivalent to solve the problem $\min_{q(\cdot|v_i)} \sum_{i=1}^n \mathbb{E}_{v_j \sim q(\cdot|v_i)} \hat{d}_{ij} - H_i(v)$ where $H_i(v) = -\sum_{j=1}^n q(v_j|v_i) \log q(v_j|v_i)$ represents the entropy of the connectivity distribution of node v_i .

3.4. Spectral Analysis

As mentioned in the above subsection, AdaGAE generates a weighted graph with adaptive self-loops. Analogous to SGC [36], Theorem 4 shows that adaptive self-loops also reduce the spectrum of the normalized Laplacian, i.e., it smooths the Laplacian.

Theorem 4. Let $\tilde{A}' = \tilde{A} - \text{diag}(\tilde{A})$ and $\hat{A}' = \tilde{D}'^{-\frac{1}{2}} \tilde{A}' \tilde{D}'^{-\frac{1}{2}}$. According to eigenvalue decomposition, suppose $I - \hat{A} = Q \Lambda Q^T$ and $I - \hat{A}' = Q' \Lambda' Q'^T$. The following inequality always holds

$$0 = \lambda_1 = \lambda'_1 < \lambda_n < \lambda'_n, \quad (14)$$

where λ_i and λ'_i denote the i -th smallest eigenvalue of $I - \hat{A}$ and $I - \hat{A}'$, respectively.

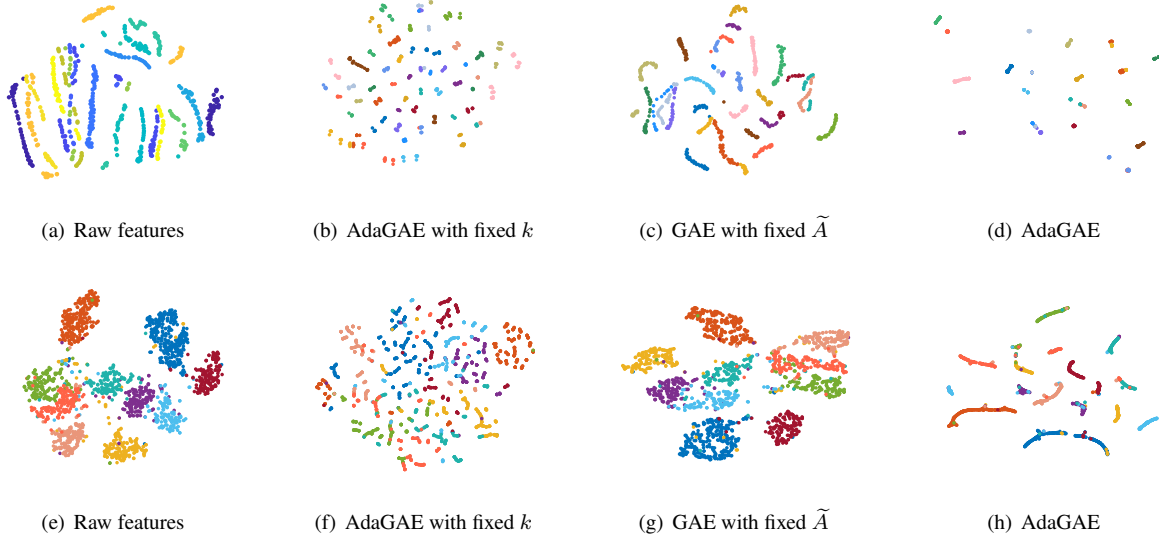


Figure 3. t-SNE visualization on UMIST and USPS: The first and second line illustrate results on UMIST and USPS, respectively. Clearly, AdaGAE projects most semblable samples into the analogous embedding. Note that the cohesive embedding is preferable for clustering.

3.5. Computational Complexity

In the phase of training GCN, the most time-consuming operation is to compute $\hat{A}T_i$ where $T_i = XW_i \in \mathbb{R}^{n \times d_i}$. Since \hat{A} is sparse, the amount of non-zero entries is denoted by $|\mathcal{E}|$. Therefore, the computational complexity of each iteration to update GCN is $O(|\mathcal{E}|d_i)$. To construct the graph matrix, A , $O(n^2)$ time is required which is same with the spectral clustering. After the embedding is obtained, the complexity to get clustering assignments is $O(n^2c)$ (using the spectral clustering) or $O(ndc)$ (using k -means).

3.6. Optimization of Problem (21)

To keep notations uncluttered, $p(v_j|v_i)$ is simplified as p_{ij} . Then the problem (21) is equivalent to solve the following subproblem individually

$$\min_{\mathbf{p}^T \mathbf{1}=1, \mathbf{p} \geq 0} \sum_{j=1}^n p_{ij} d_{ij} + \gamma \|\mathbf{p}_i\|_2^2. \quad (15)$$

To keep the discussion more concise, the subscript i is neglected. Due to d_j is constant, we have

$$\min_{\mathbf{p}^T \mathbf{1}=1, \mathbf{p} \geq 0} \sum_{j=1}^n p_j d_j + \gamma \|\mathbf{p}\|_2^2 \Leftrightarrow \min_{\mathbf{p}^T \mathbf{1}=1, \mathbf{p} \geq 0} \left\| \mathbf{p} + \frac{\mathbf{d}}{2\gamma} \right\|_2^2. \quad (16)$$

Then the Lagrangian of the above equation is

$$\mathcal{L} = \left\| \mathbf{p} + \frac{\mathbf{d}}{2\gamma} \right\|_2^2 + \alpha \left(1 - \sum_{j=1}^n p_j \right) + \sum_{j=1}^n \beta_j (-p_j), \quad (17)$$

where α and β_j are the Lagrange multipliers. According to the KKT conditions, we have

$$\begin{cases} p_j + \frac{d_j}{2\gamma} - \alpha - \beta_j = 0 \\ \beta_j p_j = 0, \beta_j \geq 0 \\ \sum_{j=1}^n p_j = 1, p_j \geq 0 \end{cases} \Rightarrow p_j = \left(\alpha - \frac{d_j}{2\gamma} \right)_+, \quad (18)$$

where $(\cdot)_+ = \max(\cdot, 0)$. Without loss of generality, suppose that $d_1 \leq d_2 \leq \dots \leq d_n$. According to Theorem 5, $\|\mathbf{p}\|_0 = k$, or equivalently, $\alpha - \frac{d_{k+1}}{2\gamma} \leq 0 < \alpha - \frac{d_k}{2\gamma}$ where $k \in [1, n)$. Due to $\mathbf{p}^T \mathbf{1} = 1$, we have

$$\alpha = \frac{1}{k} \left(1 + \sum_{j=1}^k \frac{d_j}{2\gamma} \right). \quad (19)$$

Substitute Eq. (7) into Eq. (19), and we have

$$p_j = \left(\frac{d_{k+1} - d_j}{\sum_{j=1}^k (d_{k+1} - d_j)} \right)_+. \quad (20)$$

If $k \geq n$, then it is not hard to verify that Eq. (20) is also the optima. Accordingly, the connectivity distribution can be calculated via closed-form solutions.

4. Experiments

In this section, details of AdaGAE are demonstrated and the results are shown. The visualization supports the theoretical analyses mentioned in the last section.

4.1. Datasets and Compared Methods

AdaGAE is evaluated on 10 datasets of different types, including 2 text datasets (*Text* and *20news*), 3 UCI [7]

Table 1. ACC (%)

Methods	Text	20news	Isolet	Segment	PALM	UMIST	JAFPE	COIL20	USPS	MNIST
K-Means	86.34	25.26	59.11	54.97	70.39	42.87	72.39	58.26	64.67	55.87
CAN	50.31	25.39	61.47	49.13	88.10	<u>69.62</u>	<u>96.71</u>	84.10	67.96	74.85
RCut	53.44	28.06	<u>65.96</u>	43.23	61.36	61.31	83.62	69.57	63.86	63.52
NCut	55.34	31.26	60.06	51.74	61.19	60.05	80.44	70.28	63.50	64.90
DEC	50.62	25.11	34.17	14.29	27.45	36.47	62.95	74.35	42.30	81.22
DFKM	52.77	29.65	51.99	51.47	67.45	45.47	90.83	60.21	73.42	48.37
GAE	53.45	25.59	61.41	<u>60.43</u>	<u>88.45</u>	61.91	94.37	69.10	<u>76.63</u>	70.22
MGAE	50.48	<u>41.47</u>	46.31	50.44	51.47	49.19	87.22	60.99	64.13	55.17
GALA	50.31	28.16	53.59	49.57	79.45	41.39	94.37	80.00	67.64	74.26
SDCN	55.70	31.06	57.56	50.95	27.75	27.65	33.80	41.04	37.43	66.85
SpectralNet	48.20	25.37	52.98	51.39	88.30	52.53	88.26	75.63	70.93	<u>82.10</u>
GAE [†]	50.31	33.55	62.05	47.66	82.10	72.17	96.71	85.97	79.40	71.07
Method-A	50.00	38.54	66.15	41.13	88.30	73.22	96.71	92.43	67.48	73.87
Method-B	51.13	33.35	54.49	38.66	91.80	32.00	47.42	33.82	34.09	14.04
AdaGAE	89.31	77.28	66.22	60.95	95.25	83.48	97.27	93.75	91.96	92.88

datasets (*Isolet*, *Segment*, and *PALM*), and 5 image datasets (*UMIST* [13], *JAFPE* [18], *COIL20* [20], *USPS* [14], and *MNIST-test* [17]). Note that USPS used in our experiments is a subset with 1854 samples of the whole dataset. To keep notations simple, MNIST-test is denoted by *MNIST*. Note that all features are rescaled to $[0, 1]$. The details of these datasets are shown in supplementary.

To evaluate the performance of AdaGAE, 11 methods serve as competitors. To ensure the fairness, 4 clustering methods without neural networks are used, including *K-Means*, *CAN* [22], Ratio Cut (*RCut*) [10], and Normalized Cut (*NCut*) [21]. Three deep clustering methods for general data, *DEC* [37], *DFKM* [41], and *SpectralNet* [30], also serve as an important baseline. Besides, four GAE-based methods are used, including *GAE* [15], *MGAE* [33], *GALA* [25], and *SDCN* [2]. All codes are downloaded from the homepages of authors. The concrete information of their settings can be found in supplementary.

4.2. Experimental Setup

In our experiments, the encoder consists of two GCN layers. If the input dimension is 1024, the first layer has 256 neurons and the second layer has 64 neurons. Otherwise, the two layers have 128 neurons and 64 neurons respectively. The activation function of the first layer is set as ReLU while the other one employs the linear function. The initial sparsity k_0 is set as 5 and the upper bound k_m is searched from $\{\lfloor \frac{n}{c} \rfloor, \lfloor \frac{n}{2c} \rfloor\}$. The tradeoff coefficient λ is searched from $\{10^{-3}, 10^{-2}, \dots, 10^3\}$. The number of graph update step is set as 10 and the maximum iterations to optimize GAE varies in $[150, 200]$.

To study the roles of different parts, the ablation experiments are conducted: GAE with $\lambda = 0$ and fixed \tilde{A}

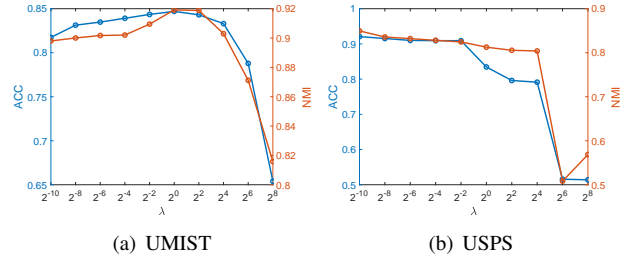


Figure 4. Parameter sensitivity of λ on UMIST and USPS. On UMIST, the second term improves the performance distinctly. Besides, if λ is not too large, AdaGAE will obtain good results.

(denoted by *GAE*[†]), AdaGAE with fixed \tilde{A} (denoted by *Method-A*), and AdaGAE with fixed sparsity k (denoted by *Method-B*).

Two popular clustering metrics, the clustering accuracy (ACC) and normalized mutual information (NMI), are employed to evaluate the performance. All methods are run 10 times and the means are reported. The code of AdaGAE is implemented under pytorch-1.3.1 on a PC with an NVIDIA GeForce GTX 1660 GPU. The exact settings of all methods can be found in supplementary.

4.3. Experimental Results

To illustrate the process of AdaGAE, Figure 2 shows the learned embedding on USPS at the i -th epoch. An epoch means a complete training of GAE and an update of the graph. The maximum number of epochs, T , is set as 10. In other words, the graph is constructed 10 times. Clearly, the embedding becomes more cohesive with the update.

ACCs and NMIs of all methods are reported in Table 1 and 2. The best results of both competitors and AdaGAEs are highlighted in boldface while the suboptimal results are

Table 2. NMI (%)

Methods	Text	20news	Isolet	Segment	PALM	UMIST	JAFPE	COIL20	USPS	MNIST
K-Means	<u>51.09</u>	0.27	74.15	55.40	89.98	65.47	80.90	74.58	62.88	54.17
CAN	2.09	3.41	78.17	52.62	<u>97.08</u>	<u>87.75</u>	<u>96.39</u>	<u>90.93</u>	<u>78.85</u>	77.30
RCut	0.35	4.59	<u>78.55</u>	53.22	85.78	77.64	90.63	84.16	70.35	70.29
NCut	0.93	4.57	72.11	51.11	85.21	77.54	89.56	84.70	70.43	72.15
DEC	2.09	0.27	70.13	0.00	55.22	56.96	82.83	90.37	48.71	<u>80.25</u>
DFKM	0.25	3.39	69.81	49.91	86.74	67.04	92.01	76.81	71.58	38.75
GAE	35.63	4.49	74.63	50.22	94.87	80.24	93.26	86.45	76.02	65.58
MGAE	1.40	<u>23.41</u>	65.06	39.26	81.13	68.00	89.65	73.59	62.18	57.33
GALA	2.09	3.09	71.60	<u>57.09</u>	89.50	63.71	92.54	87.71	71.50	75.65
SDCN	0.94	1.71	73.05	45.89	60.18	38.65	46.85	60.07	38.97	69.14
SpectralNet	3.77	3.45	78.60	53.64	92.87	79.99	87.02	88.00	74.84	<u>81.70</u>
GAE [†]	2.09	10.30	78.61	53.86	93.86	87.00	96.39	95.62	78.46	76.15
Method-A	0.52	25.18	79.76	52.16	96.96	87.04	96.39	97.26	76.45	76.59
Method-B	0.14	6.38	77.70	30.02	97.80	52.08	59.55	55.46	35.39	1.63
AdaGAE	51.59	49.60	78.89	59.76	98.18	91.03	96.78	98.36	84.81	85.31

underlined. From Table 1 and 2, we conclude that:

- On text datasets (Text and 20news), most graph-based methods get a trivial result, as they group all samples into the same cluster such that NMIs approximate 0. Only k -means, MGAE, and AdaGAE obtain the non-trivial assignments.
- Classical clustering models work poorly on large scale datasets. Instead, DEC and SpectralNet work better on the large scale datasets. Although GAE-based models (GAE, MGAE, and GALA) achieve impressive results on graph type datasets, they fail on the general datasets, which is probably caused by the fact that the graph is constructed by an algorithm rather than prior information. If the graph is not updated, the contained information is low-level. The adaptive learning will induce the model to exploit the high-level information. In particular, AdaGAE is stable on all datasets.
- When the sparsity k keeps fixed, AdaGAE collapses on most of datasets. For example, ACC shrinks about 50% and NMI shrinks about 40% on COIL20.
- From the comparison of 3 extra experiments, we confirm that the adaptive graph update plays a positive role. Besides, the novel architecture with weighted graph improves the performance on most of datasets.

To study the impact of different parts of the loss in Eq. (11), the performance with different λ is reported in Figure 4. From it, we find that the second term (corresponding to problem (21)) plays an important role especially on UMIST. If λ is set as a large value, we may get the trivial embedding according to the constructed graph. AdaGAE will obtain good results when λ is not too large.

Besides, Figure 5 illustrates the learned embedding vividly. Combining with Theorem 2, if k is fixed, then \tilde{A} degenerates into an unweighted adjacency matrix and a cluster is broken into a mass of groups. Each group only contains a small number of data points and they scatter chaotically, which leads to collapse. Instead, *the adaptive process connects these groups before degeneration via increasing sparsity k , and hence, the embeddings in a cluster become cohesive*. Note that **the cohesive representations are preferable (not over-fitting) for clustering due to the unsupervised setting**. It should be emphasized that a large k_0 frequently leads to capture the wrong information. After the transformation of GAE, the nearest neighbors are more likely to belong with the same cluster and thus it is rational to increasing k with an adequate step size.

5. Conclusion

In this paper, we propose a novel clustering model for general data clustering, namely Adaptive Graph Auto-Encoder (*AdaGAE*). A generative graph representation model is utilized to construct a weighted graph with steerable sparsity. To exploit potential information, we employ a graph auto-encoder to exploit the high-level information. As the graph used in GAE is constructed artificially, an adaptive update step is developed to update the graph with the help of learned embedding. Related theoretical analyses demonstrate the reason why AdaGAE with fixed sparsity collapses in the update step such that a dynamic sparsity is essential. In experiments, we show the significant performance of AdaGAE and verify the effectiveness of the adaptive update step via the ablation experiments. Surprisingly, the visualization supports the theoretical analysis well and helps to understand how AdaGAE works.

References

- [1] Sami Abu-El-Haija, Bryan Perozzi, Amol Kapoor, Nazanin Alipourfard, Kristina Lerman, Hrayr Harutyunyan, Greg Ver Steeg, and Aram Galstyan. Mixhop: Higher-order graph convolutional architectures via sparsified neighborhood mixing. In *International Conference on Machine Learning*, pages 21–29, 2019. 2
- [2] Deyu Bo, Xiao Wang, Chuan Shi, Meiqi Zhu, Emiao Lu, and Peng Cui. Structural deep clustering network. In *WWW*, pages 1400–1410. ACM / IW3C2, 2020. 7
- [3] Joan Bruna, Wojciech Zaremba, Arthur Szlam, and Yann LeCun. Spectral networks and locally connected networks on graphs. *arXiv preprint arXiv:1312.6203*, 2013. 2
- [4] Shaosheng Cao, Wei Lu, and Qiongkai Xu. Deep neural networks for learning graph representations. In *Thirtieth AAAI conference on artificial intelligence*, 2016. 1
- [5] Jianfei Chen, Jun Zhu, and Le Song. Stochastic training of graph convolutional networks with variance reduction. In *International Conference on Machine Learning*, pages 942–950, 2018. 3
- [6] Wei-Lin Chiang, Xuanqing Liu, Si Si, Yang Li, Samy Bengio, and Cho-Jui Hsieh. Cluster-gcn: An efficient algorithm for training deep and large graph convolutional networks. In *Proceedings of the 25th ACM SIGKDD International Conference on Knowledge Discovery & Data Mining*, pages 257–266, 2019. 3
- [7] Dheeru Dua and Casey Graff. UCI machine learning repository, 2017. 6
- [8] Kamran Ghasedi Dizaji, Amirhossein Herandi, Cheng Deng, Weidong Cai, and Heng Huang. Deep clustering via joint convolutional autoencoder embedding and relative entropy minimization. In *Proceedings of the IEEE international conference on computer vision*, pages 5736–5745, 2017. 1, 2
- [9] Aditya Grover and Jure Leskovec. node2vec: Scalable feature learning for networks. In *Proceedings of the 22nd ACM SIGKDD international conference on Knowledge discovery and data mining*, pages 855–864, 2016. 1
- [10] Lars Hagen and Andrew B Kahng. New spectral methods for ratio cut partitioning and clustering. *IEEE transactions on computer-aided design of integrated circuits and systems*, 11(9):1074–1085, 1992. 7
- [11] Xiaofei He and Partha Niyogi. Locality preserving projections. In *Advances in Neural Information Processing Systems 16*, pages 153–160. 2004. 3
- [12] G. E Hinton and R. Salakhutdinov. Reducing the dimensionality of data with neural networks. *Science*, 313(5786):504–507, 2006. 2
- [13] C. Hou, F. Nie, X. Li, D. Yi, and Y. Wu. Joint embedding learning and sparse regression: A framework for unsupervised feature selection. *IEEE Transactions on Cybernetics*, 44(6):793–804, 2013. 7
- [14] J. Hull. A database for handwritten text recognition research. *IEEE Transactions on Pattern Analysis and Machine Intelligence*, 16(5):550–554, 1994. 7
- [15] Thomas N Kipf and Max Welling. Variational graph autoencoders. *arXiv preprint arXiv:1611.07308*, 2016. 1, 3, 7
- [16] Thomas N Kipf and Max Welling. Semi-supervised classification with graph convolutional networks. In *ICLR*, 2017. 2, 4
- [17] Y. LeCun. The mnist database of handwritten digits, 1998. 7
- [18] M. Lyons, J. Budynek, and S. Akamatsu. Automatic classification of single facial images. *IEEE transactions on pattern analysis and machine intelligence*, 21(12):1357–1362, 1999. 7
- [19] Alireza Makhzani, Jonathon Shlens, Navdeep Jaitly, Ian Goodfellow, and Brendan Frey. Adversarial autoencoders. *arXiv preprint arXiv:1511.05644*, 2015. 2
- [20] S. Nene, S. Nayar, and H. Murase. Columbia object image library (coil-20). 1996. 7
- [21] Andrew Y Ng, Michael I Jordan, and Yair Weiss. On spectral clustering: Analysis and an algorithm. In *Advances in neural information processing systems*, pages 849–856, 2002. 1, 7
- [22] Feiping Nie, Xiaoqian Wang, and Heng Huang. Clustering and projected clustering with adaptive neighbors. In *Proceedings of the 20th ACM SIGKDD international conference on Knowledge discovery and data mining*, pages 977–986. ACM, 2014. 1, 7
- [23] Mathias Niepert, Mohamed Ahmed, and Konstantin Kutikov. Learning convolutional neural networks for graphs. In *International conference on machine learning*, pages 2014–2023, 2016. 2
- [24] Shirui Pan, Ruiqi Hu, Guodong Long, Jing Jiang, Lina Yao, and Chengqi Zhang. Adversarially regularized graph autoencoder for graph embedding. In *IJCAI*, pages 2609–2615, 2018. 3
- [25] Jiwoong Park, Minsik Lee, Hyung Jin Chang, Kyuewang Lee, and Jin Young Choi. Symmetric graph convolutional autoencoder for unsupervised graph representation learning. In *Proceedings of the IEEE International Conference on Computer Vision*, pages 6519–6528, 2019. 7
- [26] Xi Peng, Jiashi Feng, Shijie Xiao, Wei-Yun Yau, Joey Tianyi Zhou, and Songfan Yang. Structured autoencoders for subspace clustering. *IEEE Transactions on Image Processing*, 27(10):5076–5086, 2018. 2
- [27] Bryan Perozzi, Rami Al-Rfou, and Steven Skiena. Deepwalk: Online learning of social representations. In *Proceedings of the 20th ACM SIGKDD international conference on Knowledge discovery and data mining*, pages 701–710. ACM, 2014. 1
- [28] S T Roweis and L K Saul. Nonlinear dimensionality reduction by locally linear embedding. *Science*, 290(5500):2323–2326, 2000. 3
- [29] Franco Scarselli, Marco Gori, Ah Chung Tsoi, Markus Hagenbuchner, and Gabriele Monfardini. The graph neural network model. *IEEE Transactions on Neural Networks*, 20(1):61–80, 2008. 1
- [30] Uri Shaham, Kelly Stanton, Henry Li, Boaz Nadler, Ronen Basri, and Yuval Kluger. Spectralnet: Spectral clustering using deep neural networks. *arXiv preprint arXiv:1801.01587*, 2018. 1, 2, 7
- [31] J B Tenenbaum, De Silva, V, and J C Langford. A global geometric framework for nonlinear dimensionality reduction. *Science*, 290(5500):2319–2323, 2000. 3

- [32] Chun Wang, Shirui Pan, Ruiqi Hu, Guodong Long, Jing Jiang, and Chengqi Zhang. Attributed graph clustering: a deep attentional embedding approach. In *Proceedings of the 28th International Joint Conference on Artificial Intelligence*, pages 3670–3676. AAAI Press, 2019. [3](#)
- [33] Chun Wang, Shirui Pan, Guodong Long, Xingquan Zhu, and Jing Jiang. Mgae: Marginalized graph autoencoder for graph clustering. In *Proceedings of the 2017 ACM on Conference on Information and Knowledge Management*, pages 889–898, 2017. [3](#), [7](#)
- [34] Daixin Wang, Peng Cui, and Wenwu Zhu. Structural deep network embedding. In *Proceedings of the 22nd ACM SIGKDD international conference on Knowledge discovery and data mining*, pages 1225–1234, 2016. [1](#)
- [35] Hongwei Wang, Jia Wang, Jialin Wang, Miao Zhao, Weinan Zhang, Fuzheng Zhang, Xing Xie, and Minyi Guo. Graphgan: Graph representation learning with generative adversarial nets. In *Thirty-Second AAAI Conference on Artificial Intelligence*, pages 2508–2515, 2018. [1](#)
- [36] Felix Wu, Tianyi Zhang, Amaur Holanda de Souza, Christopher Fifty, Tao Yu, and Kilian Q Weinberger. Simplifying graph convolutional networks. *Proceedings of Machine Learning Research*, 2019. [2](#), [5](#), [12](#)
- [37] Junyuan Xie, Ross Girshick, and Ali Farhadi. Unsupervised deep embedding for clustering analysis. In *International conference on machine learning*, pages 478–487, 2016. [1](#), [2](#), [7](#)
- [38] Keyulu Xu, Weihua Hu, Jure Leskovec, and Stefanie Jegelka. How powerful are graph neural networks? In *Proc. of ICLR*, 2019. [2](#)
- [39] Jianwei Yang, Devi Parikh, and Dhruv Batra. Joint unsupervised learning of deep representations and image clusters. In *Proceedings of the IEEE Conference on Computer Vision and Pattern Recognition*, pages 5147–5156, 2016. [1](#), [2](#)
- [40] Xu Yang, Cheng Deng, Feng Zheng, Junchi Yan, and Wei Liu. Deep spectral clustering using dual autoencoder network. In *Proceedings of the IEEE Conference on Computer Vision and Pattern Recognition*, pages 4066–4075, 2019. [1](#), [2](#)
- [41] R. Zhang, X. Li, H. Zhang, and F. Nie. Deep fuzzy k-means with adaptive loss and entropy regularization. *IEEE Transactions on Fuzzy Systems*, pages 1–1, 2019. [1](#), [2](#), [7](#)
- [42] Rui Zhang, Feiping Nie, Muhan Guo, Xian Wei, and Xuelong Li. Joint learning of fuzzy k-means and nonnegative spectral clustering with side information. *IEEE Transactions on Image Processing*, 28(5):2152–2162, 2018. [1](#)

A. Proof of Theorem 1

Theorem 5. The ℓ_2 -norm relaxation of the original problem,

$$\min_{p(\cdot|v_i)} \sum_{i=1}^n \mathbb{E}_{v_j \sim p(\cdot|v_i)} d_{ij} + \gamma_i \|\mathbf{p}_i\|_2^2, \quad (21)$$

has a k -sparse solution if γ_i satisfies

$$\frac{1}{2}(kd_{i\cdot}^{(k)} - \sum_{v=1}^k d_{i\cdot}^{(v)}) < \gamma_i \leq \frac{1}{2}(kd_{i\cdot}^{(k+1)} - \sum_{v=1}^k d_{i\cdot}^{(v)}). \quad (22)$$

where $d_{i\cdot}^{(v)}$ denotes the v -th smallest value of $\{d_{ij}\}_{j=1}^n$.

Proof. The problem to optimize is equivalent to the following subproblem

$$\min_{\mathbf{p}^T \mathbf{1}=1, \mathbf{p} \geq 0} \|\mathbf{p} + \frac{\mathbf{d}}{2\gamma}\|_2^2, \quad (23)$$

where the subscript i is ignored. According to the KKT conditions, we have

$$\begin{cases} p_j + \frac{d_j}{2\gamma} - \alpha - \beta_j = 0 \\ \beta_j p_j = 0, \beta_j \geq 0 \\ \sum_{j=1}^n p_j = 1, p_j \geq 0 \end{cases} \Rightarrow p_j = (\alpha - \frac{d_j}{2\gamma})_+. \quad (24)$$

Note that the auxiliary function,

$$f(x) = (C_1 - \frac{C_2}{2x})_+, \forall C_2 > 0, \quad (25)$$

is non-decreasing with x . Note that $f(x)$ is strictly increasing when $2x \geq C_2$. If $\alpha \in [\frac{d_1}{2\gamma}, \frac{d_n}{2\gamma}]$, there must exist m that satisfies $\alpha - \frac{d_{m+1}}{2\gamma} \leq 0 < \alpha - \frac{d_m}{2\gamma}$. In this case, \mathbf{p} is m -sparse. According to Eq. (24), we have

$$\alpha = \frac{1}{m}(1 + \sum_{j=1}^m \frac{d_j}{2\gamma}) \Rightarrow p_j = \frac{1}{m}(1 - \frac{\sum_{i=1}^m (d_j - d_i)}{2\gamma})_+. \quad (26)$$

When γ satisfies Eq. (22), we have

$$\frac{1}{m}(1 - \frac{\sum_{i=1}^m (d_j - d_i)}{\sum_{i=1}^k (d_k - d_i)})_+ \leq p_j \leq \frac{1}{m}(1 - \frac{\sum_{i=1}^m (d_j - d_i)}{\sum_{i=1}^k (d_{k+1} - d_i)})_+, \quad (27)$$

according to the non-decreasing property of the auxiliary function $f(x)$. If $m > k$, then

$$0 \leq p_m \leq \frac{1}{m}(1 - \frac{\sum_{i=1}^m (d_m - d_i)}{\sum_{i=1}^k (d_{k+1} - d_i)})_+ \leq 0. \quad (28)$$

Hence, $p_m = 0$ which leads to contradiction. If $m < k$

$$p_{m+1} > \frac{1}{m}(1 - \frac{\sum_{i=1}^m (d_{m+1} - d_i)}{\sum_{i=1}^k (d_k - d_i)})_+ > 0. \quad (29)$$

In the first inequality, the equality will never hold due to $2\gamma > \sum_{i=1}^k (d_k - d_i) \geq \sum_{i=1}^k (d_{m+1} - d_i)$. Accordingly, \mathbf{p} is at least $(m+1)$ -sparse, which lead to contradiction as well. Therefore, we have $k = m$.

When $(\frac{d_n}{2\gamma}, +\infty)$, it is not hard to verify that $p_m = 0$ which also leads to contradiction. Finally, $\alpha \in (-\infty, \frac{d_1}{2\gamma})$ will never hold due to the constraint $\mathbf{p}^T \mathbf{1} = 1$.

In sum, the theorem is proved. \square

B. Proof of Theorem 2

Proof of Theorem 2. Without loss of generality, we focus on the connectivity distribution of v and suppose that $p(v_1|v) \geq p(v_2|v) \geq \dots \geq p(v_k|v) > 0 = p(v_{k+1}|v) = \dots = p(v_n|v)$. Let $p_i = p(v_i|v)$ and $q_i = q(v_i|v)$. According to the definitions,

$$\begin{cases} p_i = \frac{d_{k+1} - d_i}{\sum_{j=1}^k (d_{k+1} - d_j)} \\ q_i = \frac{\exp(-\hat{d}_i)}{\sum_{j=1}^n \exp(-\hat{d}_j)}. \end{cases} \quad (30)$$

If for any i , we have $|p_i - q_i| \leq \varepsilon$. Clearly, $p_{k+1} = 0$. Suppose that $q_{k+1} = \tau \leq \varepsilon$. Therefore, we have

$$\begin{aligned} \frac{\exp(-\hat{d}_{k+1})}{\sum_{j=1}^n \exp(-\hat{d}_j)} &= \tau \\ \Leftrightarrow \hat{d}_{k+1} &= \log \frac{1}{\tau} - \log C. \end{aligned} \quad (31)$$

where $C = \sum_{j=1}^n \exp(-\hat{d}_j)$. Combine with the condition, $p_k \geq \sqrt{\varepsilon}$, and we have

$$\begin{aligned} \frac{\exp(-\hat{d}_k)}{\sum_{j=1}^n \exp(-\hat{d}_j)} &\geq p_k - \varepsilon \geq \sqrt{\varepsilon} - \varepsilon \\ \Rightarrow \hat{d}_k &\leq -\log C - \log(\sqrt{\varepsilon} - \varepsilon). \end{aligned} \quad (32)$$

Similarly, since $p_1 \geq 1/k$,

$$\begin{aligned} \frac{\exp(-\hat{d}_1)}{\sum_{j=1}^n \exp(-\hat{d}_j)} &\leq 1 \\ \Rightarrow \hat{d}_1 &\geq -\log C. \end{aligned} \quad (33)$$

If we update the connectivity distribution based on $\{\hat{d}_i\}_{i=1}^n$, then for any $i \leq k$,

$$\hat{p}_i = \frac{\hat{d}_{k+1} - \hat{d}_i}{\sum_{j=1}^k (\hat{d}_{k+1} - \hat{d}_j)}. \quad (34)$$

Furthermore, for any $i, j \leq k$,

$$\begin{aligned}
|\hat{p}_i - \hat{p}_j| &= \frac{|\hat{d}_j - \hat{d}_i|}{\sum_{j=1}^k (\hat{d}_{k+1} - \hat{d}_j)} \\
&\leq \frac{|\hat{d}_k - \hat{d}_1|}{\sum_{j=1}^k (\hat{d}_{k+1} - \hat{d}_j)} \\
&= \frac{-\log(\sqrt{\varepsilon} - \varepsilon)}{\sum_{j=1}^k (\log \frac{1}{\tau} - \log C - \hat{d}_j)} \\
&\leq \frac{-\log(\sqrt{\varepsilon} - \varepsilon)}{\sum_{j=1}^k (\log \frac{1}{\tau} - \log C - \hat{d}_k)} \quad (35) \\
&\leq \frac{-\log(\sqrt{\varepsilon} - \varepsilon)}{k(\log(\sqrt{\varepsilon} - \varepsilon) - \log \tau)} \\
&= \frac{1}{k} \cdot \frac{\log(\sqrt{\varepsilon} - \varepsilon)}{\log \tau - \log(\sqrt{\varepsilon} - \varepsilon)} \\
&= \frac{1}{k} \cdot \frac{1}{\frac{\log \tau}{\log(\sqrt{\varepsilon} - \varepsilon)} - 1} \\
&\leq \frac{1}{k} \cdot \frac{1}{\frac{\log \varepsilon}{\log(\sqrt{\varepsilon} - \varepsilon)} - 1}.
\end{aligned}$$

With $\varepsilon \rightarrow 0$, $|\hat{p}_i - \hat{p}_j| \rightarrow 0$.

The proof is easy to extend to other nodes. Hence, the theorem is proved. \square

C. Proof of Theorem 3

Proof of Theorem 3. The problem,

$$\min_{q(\cdot|v_i)} \sum_{i=1}^n \mathbb{E}_{v_j \sim q(\cdot|v_i)} \hat{d}_{ij} - H_i(v), \quad (36)$$

is equivalent to the following i -th subproblem

$$\begin{aligned}
&\min_{q_{ij}} \sum_{j=1}^n q_{ij} \hat{d}_{ij} + q_{ij} \log q_{ij}, \\
&s.t. \sum_{j=1}^n q_{ij} = 1, q_{ij} > 0.
\end{aligned} \quad (37)$$

Similarly, the subscript i is omitted to keep notations uncluttered. The Lagrangian is

$$\mathcal{L} = \sum_{j=1}^n q_j \hat{d}_j + q_j \log q_j + \alpha(1 - \sum_{j=1}^n q_j) + \sum_{j=1}^n \beta_j(-q_j). \quad (38)$$

Then the KKT conditions are

$$\begin{cases} \hat{d}_j + 1 + \log q_j - \alpha - \beta_j &= 0 \\ 1 - \sum_{j=1}^n q_j &= 0 \\ \beta_j q_j &= 0 \\ \beta_j &\geq 0. \end{cases} \quad (39)$$

Due to $q_j > 0$, $\beta_j = 0$. Use the first line, we have

$$q_j = \exp(\alpha - \hat{d}_j - 1). \quad (40)$$

Combine it with the second line and we have

$$\exp(\alpha) \sum_{j=1}^n \exp(-\hat{d}_j - 1) = 1. \quad (41)$$

Furthermore, we have

$$q_j = \frac{\exp(-\hat{d}_j - 1)}{\sum_{j=1}^n \exp(-\hat{d}_j - 1)} = \frac{\exp(-\hat{d}_j)}{\sum_{j=1}^n \exp(-\hat{d}_j)}. \quad (42)$$

With $\hat{d}_{ij} = \|z_i - z_j\|_2$, the theorem is proved. \square

D. Proof of Theorem 4

It should be pointed out that the proof imitates the corresponding proof in [36]. Analogous to Lemma 3 in [36], we first give the following lemma without proof.

Lemma 1. Let $\alpha_1 \leq \alpha_2 \leq \dots \leq \alpha_n$ be eigenvalues of $\hat{D}^{-\frac{1}{2}} \hat{A}' \hat{D}^{-\frac{1}{2}}$ and $\beta_1 \leq \beta_2 \leq \dots \leq \beta_n$ be eigenvalues of $\hat{D}'^{-\frac{1}{2}} \hat{A}' \hat{D}'^{-\frac{1}{2}}$. The following inequality always holds

$$\alpha_1 \geq \frac{\beta_1}{1 + \min \frac{\hat{A}_{ii}}{\hat{D}'_{ii}}}, \alpha_n \leq \frac{1}{1 + \max \frac{\hat{A}_{ii}}{\hat{D}'_{ii}}}. \quad (43)$$

The proof of Theorem 4 is apparent according to Lemma 3 provided in [36].

Proof of Theorem 4. Let $M = \text{diag}(\hat{A})$ and we have

$$\begin{aligned}
\lambda_n &= \max_{\|x\|=1} x^T (I - \hat{D}^{-\frac{1}{2}} M \hat{D}^{-\frac{1}{2}} - \hat{D}^{-\frac{1}{2}} \hat{A}' \hat{D}^{-\frac{1}{2}}) x \\
&\leq 1 - \min \frac{\hat{A}_{ii}}{\hat{D}'_{ii} + \hat{A}_{ii}} - \alpha_1 \\
&\leq 1 - \min \frac{\hat{A}_{ii}}{\hat{D}'_{ii} + \hat{A}_{ii}} - \frac{\beta_1}{1 + \min \frac{\hat{A}_{ii}}{\hat{D}'_{ii}}} \\
&\leq 1 - \frac{\beta_1}{1 + \min \frac{\hat{A}_{ii}}{\hat{D}'_{ii}}} \\
&\leq 1 - \beta = \lambda'_n.
\end{aligned}$$

\square

E. Experimental Details

E.1. Datasets

For all datasets, we simply rescale features into $[0, 1]$. All datasets are downloaded from <http://www.eschience.cn/people/fpnice/index.html> and <http://yann.lecun.com/exdb/mnist/>. The concrete information of them is summarized in Table 4.

Dataset	λ	k_0	γ	t_i	k_m	T	struct
Text	0.01	30	$5 * 10^{-3}$	150	$\lfloor \frac{n}{c} \rfloor$	10	d -256-64
20news	0.1	20	10^{-3}	200	$\lfloor \frac{n}{2c} \rfloor$	10	d -256-64
Isolet	0.1	20	10^{-3}	200	$\lfloor \frac{n}{c} \rfloor$	5	d -256-64
PALM	10	10	10^{-3}	50	$\lfloor \frac{n}{c} \rfloor$	10	d -256-64
UMIST	1	5	10^{-3}	50	$\lfloor \frac{n}{c} \rfloor$	10	d -256-64
COIL20	1	5	10^{-2}	100	$\lfloor \frac{n}{2c} \rfloor$	10	d -256-64
JAFFE	10^{-3}	5	10^{-2}	20	$\lfloor \frac{n}{c} \rfloor$	10	d -256-64
USPS	10^{-2}	5	5×10^{-3}	150	$\lfloor \frac{n}{c} \rfloor$	10	d -128-64
MNIST	10^{-2}	5	10^{-3}	200	$\lfloor \frac{n}{2c} \rfloor$	10	d -256-64

Table 3. λ : local information; k_0 : initial sparsity; γ : learning rate; λ : regularization coefficient; t_i : number of iterations to update GAE; struct: Neurons of each layer used in AdaGAE.

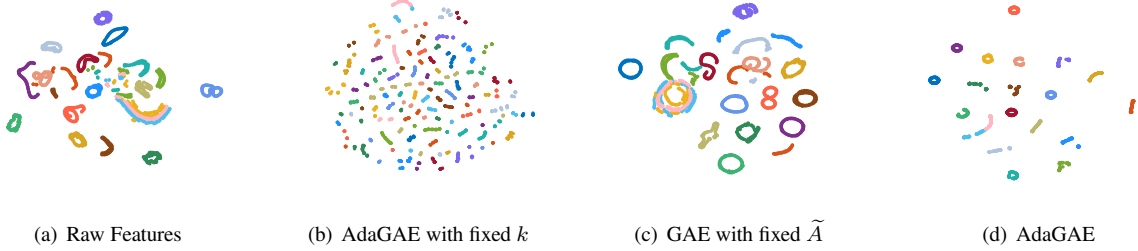


Figure 5. t-SNE visualization on COIL20.

Table 4. Information of Datasets			
Name	# Features	# Size	# Classes
Text	7511	1946	2
20news	8014	3970	4
Isolet	617	1560	26
Segment	19	2310	7
PALM	256	2000	100
UMIST	1024	575	20
JAFFE	1024	213	10
COIL20	1024	1440	20
USPS	256	1854	10
MNIST	784	10000	10

Codes of competitors are implemented under MATLAB 2019a, while codes of AdaGAE are implemented under pytorch-1.3.1-gpu. We run all experiments on a Windows PC with 8 i7 cores and a NVIDIA GeForce 1660 (6GB).

E.3. Another Visualization

The t-SNE visualization of various methods on COIL20 are shown in Figure 5. From the figure, we can find that the update of k avoid the collapse caused by the adaptive construction of the graph.

E.2. Experimental Setting

The exact values of AdaGAE in our experiments are reported in Table 3. Note that the increment t is defined as $\frac{k_m - k_0}{T}$.

To use Ratio Cut and Normalized Cut, we construct the graph via Gaussian kernel, which is given as

$$w_{ij} = \frac{\exp(-\frac{\|\mathbf{x}_i - \mathbf{x}_j\|_2}{\sigma})}{\sum_{j \in \mathcal{N}_i} \exp(-\frac{\|\mathbf{x}_i - \mathbf{x}_j\|_2}{\sigma})}, \quad (44)$$

where \mathcal{N}_i represents m -nearest neighbors of sample \mathbf{x}_i . m is searched from $\{5, 10\}$ and σ is searched from $\{10^{-3}, 10^{-2}, \dots, 10^3\}$. The maximum iterations of GAE with fixed \tilde{A} is set as 200.